

An Evaluation of Sonic IR for NDE at Lawrence Livermore National Laboratory

W. O. Miller

This article was submitted to
Thermosense XXIII Conference, Orlando, FL, April 16-20, 2001

February 1, 2001

U.S. Department of Energy

Lawrence
Livermore
National
Laboratory

DISCLAIMER

This document was prepared as an account of work sponsored by an agency of the United States Government. Neither the United States Government nor the University of California nor any of their employees, makes any warranty, express or implied, or assumes any legal liability or responsibility for the accuracy, completeness, or usefulness of any information, apparatus, product, or process disclosed, or represents that its use would not infringe privately owned rights. Reference herein to any specific commercial product, process, or service by trade name, trademark, manufacturer, or otherwise, does not necessarily constitute or imply its endorsement, recommendation, or favoring by the United States Government or the University of California. The views and opinions of authors expressed herein do not necessarily state or reflect those of the United States Government or the University of California, and shall not be used for advertising or product endorsement purposes.

This is a preprint of a paper intended for publication in a journal or proceedings. Since changes may be made before publication, this preprint is made available with the understanding that it will not be cited or reproduced without the permission of the author.

This work was performed under the auspices of the United States Department of Energy by the University of California, Lawrence Livermore National Laboratory under contract No. W-7405-Eng-48.

This report has been reproduced directly from the best available copy.

Available electronically at <http://www.doc.gov/bridge>

Available for a processing fee to U.S. Department of Energy
And its contractors in paper from
U.S. Department of Energy
Office of Scientific and Technical Information
P.O. Box 62
Oak Ridge, TN 37831-0062
Telephone: (865) 576-8401
Facsimile: (865) 576-5728
E-mail: reports@adonis.osti.gov

Available for the sale to the public from
U.S. Department of Commerce
National Technical Information Service
5285 Port Royal Road
Springfield, VA 22161
Telephone: (800) 553-6847
Facsimile: (703) 605-6900
E-mail: orders@ntis.fedworld.gov
Online ordering: <http://www.ntis.gov/ordering.htm>

OR

Lawrence Livermore National Laboratory
Technical Information Department's Digital Library
<http://www.llnl.gov/tid/Library.html>

An evaluation of Sonic IR for NDE at Lawrence Livermore National Laboratory

Wayne O. Miller*

Lawrence Livermore National Laboratory
New Technologies Engineering Division, Thermal Fluids Group

ABSTRACT

Sonic IR was evaluated as an NDE technique at LLNL using a commercial ThermoSoniX system from Indigo Systems Corp. The main effort was to detect small cracks in aluminum oxide, a dense stiff ceramic. Test coupons were made containing 0.2-mm cracks by surface grinding, 1-mm cracks by compression with a Vickers bit, and 4-mm cracks by 3-point bending. Only the 3-point bend cracks produced thermal images. Several parts shattered during testing, perhaps by being forced at resonance by the 20-kHz acoustic probe. Tests on damaged carbon composite coupons produced thermal images that were in excellent agreement with ultrasonic inspection. The composite results also showed some dependence on contact location of the acoustic probe, and on the method of support. Tests on glass with surface damage produced weak images at the pits. Tests on metal ballistic targets produced thermal images at the impact sites. Modal analyses suggest that the input frequency should be matched to the desired response, and also that forced resonance damaged some parts.

Keywords: Sonic IR, Infrared thermography, Nondestructive evaluation, Dynamics, Modal analysis

1. INTRODUCTION

The Lawrence Livermore National Laboratory (LLNL) has an active research area in methods of nondestructive evaluation (NDE). Infrared methods have been part of that effort for many years, primarily using flash heating and passive imaging. Sonic IR shows promise as a new IR NDE technique that can detect flaws, such as tightly closed cracks, that are difficult to detect with other methods. LLNL set out to evaluate Sonic IR on several materials and flaw types, and the results are presented herein.

Sonic IR is a new technique for nondestructive evaluation developed at Wayne State University.¹ The method works by dynamically exciting the part being tested with an acoustic probe that is in physical contact with the part. Any resulting differential motion across a crack face creates heat by friction, and a traditional IR camera images the temperature rise at the crack. The method has been commercialized by Indigo Systems Corp., and is available as their ThermoSoniX product.² The LLNL tests were done with a rented ThermoSoniX system.

In brief, it was found that the method and equipment used for this study were effective in certain circumstances but not in others. Some tests showed excellent indications of damage, while other tests failed to show any damage where damage was plainly evident. Several parts shattered during testing. The response was found to be modestly sensitive to the contact location of the acoustic probe and also sensitive to the type of support used for the test objects in one case.

The main effort was to see if Sonic IR could detect small cracks in aluminum oxide, a dense stiff ceramic. Three types of aluminum oxide coupons with flaws were made. First, surface grinding produced a large field of surface damage of approximately 0.2-mm closed cracks. Second, a Vickers hardness test bit was pressed into the material to produce a radial array of closed surface cracks, each approximately 1 mm long. Third, notched beams were cracked by three-point bending, producing cracks approximately 4 mm long. Only the notched beam coupons produced detectable thermal images. The inability to detect the flaws in the surface ground and Vickers coupons may be due to both inadequate spatial and temporal resolution of the IR system, and also a poor match of input forcing between the acoustic probe and the aluminum oxide parts. Additional effort to resolve this is underway. Notably, the notched beam coupons were all broken during testing. Modal

* miller99@llnl.gov; phone 1-925-424-4472; fax 1-925-422-5397; Lawrence Livermore National Laboratory, POB 808, L-140, Livermore, CA USA 94551.

analysis showed that the 20-kHz input forcing was likely driving a resonant mode in the notched beams that stressed the weakened section.

Tests were made on carbon composite tensile specimens that had been fatigued to failure. These composite coupons had been previously characterized by ultrasonic imaging. The Sonic IR images of the damage areas were clear, and in excellent agreement with the ultrasonic images. The contact location of the acoustic probe was found to have a modest effect on the image quality.

Tests were made on a large carbon composite tile that had been improperly fabricated. The tile was placed on various backing supports, and the thermal images were found to vary markedly with the support method, and in fact the images were more a dynamic response of the support than an image of damage in the tile.

Tests were made on a slab of laser glass that had spallation pits from laser-induced damage. Weak thermal images were noted at the spall sites, where the glass had fractured.

Tests were made on heavy steel plates used as high-velocity gas gun targets. Thermal images were noted at the impact zones, where the targets underwent significant plastic deformation.

2. EXPERIMENTAL PROCEDURE

The experiments were all conducted using a ThermoSoniX system from Indigo Systems Corp. A photograph of the equipment in use is shown in Figure 1. The major components include an IR camera, an acoustic probe and power source, a test stand, a PC running ThermoSoniX software, and a real-time monitor.

The camera is a Merlin Mid IR camera (3 - 5 micron, NedT < 20 mK), which acquires images at 60 Hz with a 320x256 InSb array. A 13-mm optic was used for these tests. The acoustic probe vibrates at a fixed 20 kHz frequency. The power input into the probe can be set between 0 - 400 W. The metal tip of the probe is pneumatically held against the part being tested to maintain good mechanical contact. The contact force typically varied between 20 - 60 lb_f, and could be adjusted by a pressure regulator on the test stand. The test stand has mounting fixtures for the acoustic probe and the camera, allowing flexible placement of both components. The test stand also provides the pneumatic line to the probe. Test pieces can be placed on the test stand bed, or additional jigs and fixtures can be attached to the bed to allow more options for holding parts being tested. A vise was often used to hold parts, and one is shown in Figure 1 on the test bed holding a notched beam coupon.

The PC acquires the 60-Hz images, and runs the ThermoSoniX software. The software provides controls that set the length of time the probe is active, and the total image acquisition time. The recommended starting value for the probe is 0.2 sec and this can be increased to 1.5 sec. The recommended starting value for data acquisition is 0.5 sec, with a 4-sec maximum. Notably the software includes background subtraction for image enhancement. The percentage of background subtraction can be varied, allowing weak thermal signatures to be more readily identified. The acquired image stream can be viewed as a slow-motion movie, or scanned frame-by-frame. Images can be saved in a native format or as AVI and BMP movies. The real-time monitor, which is not part of the ThermoSoniX equipment, may be attached to the camera to provide a visual reference of the camera view in addition to the smaller view in the ThermoSoniX software.

Some effort is required to tune the equipment for a specific test piece. The power and contact force of the probe are the most critical parameters to be tuned. On the advice of Indigo, these parameters were set to produce the loudest chirp, on the assumption that the audible response of the test was a good indicator of mechanical coupling between the part and probe. This was still a subjective process, and the optimal settings were found by trial and error.

Fixturing parts required some thought to avoid movement and breakage. Parts tended to move both from the steady pneumatic force holding the probe to the part, and from the dynamic load of the excitation. Both forces needed to be considered to avoid part motion during a test. The pneumatic load tended to produce overturning moments on parts held in vises and jigs. The impact of the probe as it contacts the part may also cause motion or breakage. The dynamic excitation caused parts to squirm. Note that any motion of the part produces ghosts in the images if background subtraction is used, as the reference image used for subtraction is acquired prior to the part excitation. However, many parts were sufficiently stable just resting on the test stand bed, which was covered by a rubber mat.

Fixtures were also devised to allow parts to "ring" freely under excitation. A full analysis of the dynamic coupling between the probe, the part, and the fixture was beyond the scope of this study. However, intuitively it is apparent that some of the energy input into the part will be dissipated into the fixture and test stand, so several configurations were attempted in order to avoid restricting the desired part motion. Typically this involved some form of cantilever of the part from a vise.

Indigo reported some success holding parts in lightweight clamps, which rest on the test bed. The most surprising result from this study was the effect of support on a large composite tile as described later.

An individual test is triggered by simultaneously depressing two large buttons located on the sides of the test stand (perhaps to keep the hands clear of the descending probe). This triggers a synchronized series of events. The probe descends under pneumatic force until it impacts the part. The camera takes a background image. The probe excitation is triggered, and the camera records the images during and after the excitation. The pneumatic force is released and the probe rises to the ready position. Virtual gauges in the software record the parameters of the test, and a small image area provides the video playback. The recorded images can then be viewed and enhanced in software. The entire data set can be saved for later manipulation, or exported for presentation. This process may be repeated several times to tune the parameters and adjust fixturing for best effect. Overall the process was quick and easy to do.



Figure 1. ThermoSoniX equipment in use on a notched beam specimen held in a vise.

3. EXPERIMENTAL RESULTS

The results are presented below grouped by material. These are aluminum oxide, carbon composite, glass and steel. Descriptions are provided of the test parts and the method of fixturing. All parts had flaws of some type. Thermal images are provided only if flaws were detected by the Sonic IR test.

3.1. Aluminum oxide

Aluminum oxide (Al_2O_3) is a stiff dense ceramic with Young's Modulus, $E=370$ GPa, and density, $\rho=3900$ kg/m³. It is used in applications ranging from tank armor to brewing beer. Samples were made with flaw sizes ranging from approximately 0.2 – 4.0 mm, using three different techniques

3.1.1. Surface ground coupons.

Surface grinding ceramics produces many minute cracks at the surface and just below the surface. The cracks are predominantly radial surface cracks and lateral subsurface cracks as suggested in Figure 2.³ The size of a crack is roughly twice the grit size used for grinding.⁴ These coupons were made using a drum grinder with 100-grit abrasive, which has an abrasive diameter of 0.12 - 0.15 mm. Consequently the surface cracks are approximately 0.24 – 0.30 mm deep. The coupons

were made from tiles that were 15 cm x 5 cm x 0.6 cm, and grinding was done on both surfaces. A similar tile without any grinding was reserved as an undamaged reference.

It was expected that the Sonic IR results would result in a diffuse glow over the entire surface, as the densely populated cracks would all emit a thermal signature. However, no thermal signatures were detected. The coupons were mounted in several fashions, including laying flat on the test bed and cantilevered from a vise in several orientations. The full ranges of probe input power and contact force were explored without any success. It is not yet known if the failure to detect a signal was due to the type of forcing, inadequate thermal resolution, or some other consideration.

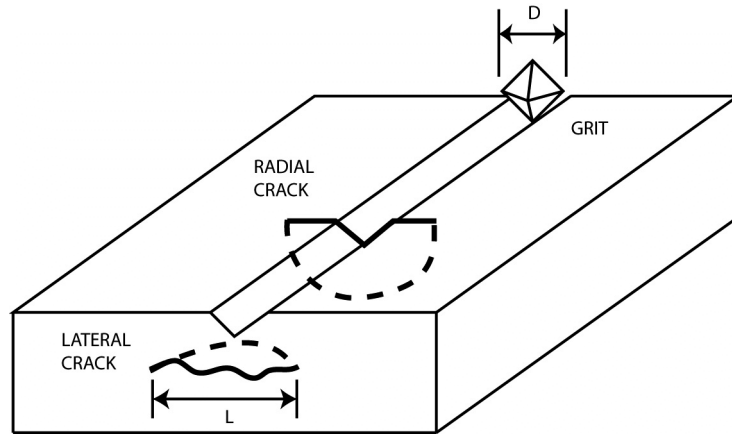


Figure 2. Schematic of damage from abrasive grinding, showing two crack modes. D is grit diameter, L is crack width, and $L \cong 2D$.

3.1.2. Vickers bit coupons.

These coupons were created by pressing a diamond-shaped Vickers hardness bit into the surface. The result is four cracks, one radiating outward from each point on the diamond as shown in Figure 3. These cracks are expected to be as deep as they are wide.⁵ The cracks shown in Figure 3 are each approximately 1 mm long, and were made using 4400 N (1000 lb_f) of compressive force applied by an MTS test machine, which applies uniaxial loads and displacements. Smaller cracks produced by lesser loads were also created. Two sizes of coupons were used for the Vickers coupons, a thick one at 10 cm x 10 cm x 2 cm, and a thin one at 15 cm x 5 cm x 0.6 cm.

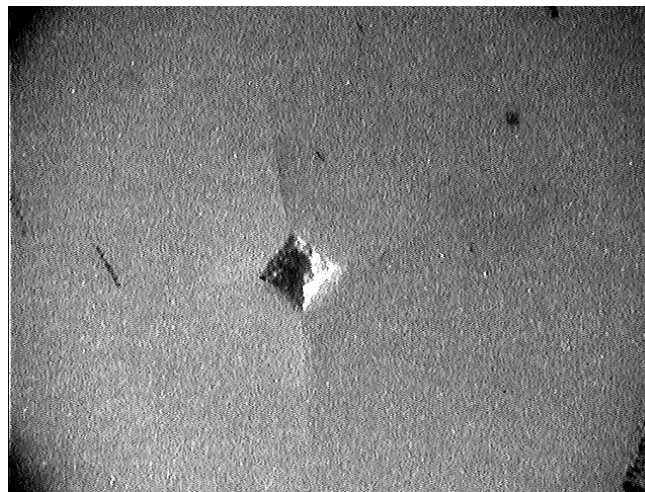


Figure 3. Photograph of Vickers bit indentation and cracks. The cracks are faintly visible as rays extending from the four points of the diamond. The cracks are approximately 1 mm long.

These cracks seemed tailor made to succeed with Sonic IR, as they are fairly large and also tightly closed. However no detectable thermal signatures were noted. The thin coupon was made after failure with the thick coupon, on the assumption that the thinner coupon would be more flexible (hence allowing more differential motion across a crack). A thinner coupon would also allow higher specific input energy due to the lower mass. Unfortunately neither coupon produced a detectable response. As with the surface ground coupons, the Vickers bit coupons were fixtured in several fashions, but with similar results in all cases.

Again, one can conjecture the failure to detect a response. One clue may be the high stiffness of aluminum oxide. This is discussed later in the section on DYNAMICS ANALYSIS, where it is shown that favorable crack-rubbing modes are at frequencies much higher than the 20-kHz probe frequency. Further, it is possible that a minute response was present, but was below the threshold of the equipment. This might be improved by a more sensitive camera or by better image enhancement algorithms. Also, aluminum oxide is fairly reflective, with an approximate emissivity of 0.4 in the 3 - 5 micron band. Better IR images might be expected with careful shrouding to reduce stray reflections, or by using a long wavelength (8-12 micron) camera, where the emissivity of aluminum oxide is 0.9.

3.1.3. Cracked beam coupons

The final aluminum oxide coupon design was a notched beam that was cracked by a bending load applied in a 3-point bend fixture. The beam design is based on a standard design for measuring fracture toughness in aluminum oxide.⁶ The beam has a chevron notch in the middle as shown in Figure 4, leaving a triangular cross section. The crack begins at the tip of the triangle, and propagates toward the base of the triangle.

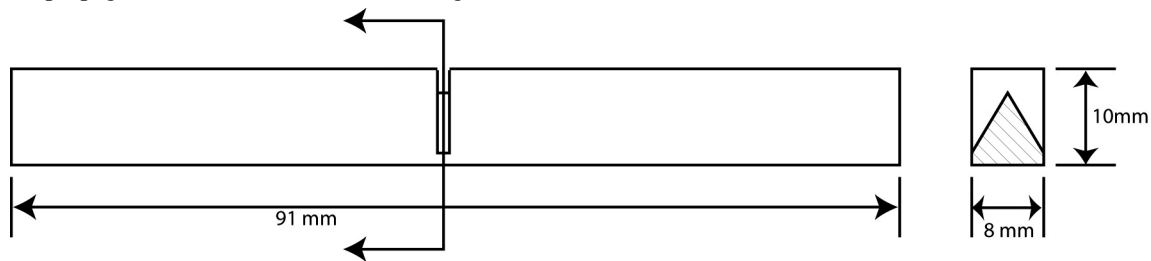


Figure 4. Notch design for cracked beam coupons.

The cracks were produced by progressively loading a beam in a 3-point bend fixture in the MTS test machine. Force and deflection were monitored, and a crack was initiated when the compressive force reached a maximum and began to decrease (Figure 5). The crack propagated with increasing deflection of the beam, and ceased when the load was removed. Direct observation of the crack was not feasible due to the notch geometry. However, the crack size was estimated by using elastic beam theory to determine an equivalent cross-section area. The cross-section area was calculated by requiring that the maximum bending stress be equal to the ultimate tensile stress of the material, subject to bending loads created by the final measured compressive force. By this technique, the crack depths were calculated to be 3.0 – 5.6 mm, depending on specimen.

The cracked beam coupons did produce thermal signatures at the notch crack. Figure 6A shows one coupon being tested. The crack thermal signature is obvious, even though the crack was not directly visible due to notch geometry. The heat generated by the Sonic IR process apparently diffused to a visible surface within a few tenths of a second. Heat is also visible at the probe contact, which was common with all tests. The cracked beam coupons were fixtured as shown in Figure 6, with one end of the beam clamped in a vise, and the probe contact near the vise jaws.

The cracked beam coupons all fractured under repeated testing, even when the probe contact force and power were reduced as low as allowable to obtain an image. Figure 6B shows the beam after the crack has completely parted the beam. The two halves of the notch are still glowing, and the unsupported half of the beam is falling towards the test bed. Thus while thermal signatures were obtained, the test was consistently destructive. An insight into the mechanism of failure is discussed below in the section on DYNAMICS ANALYSIS, where it is shown that the probe likely excited a resonant mode.

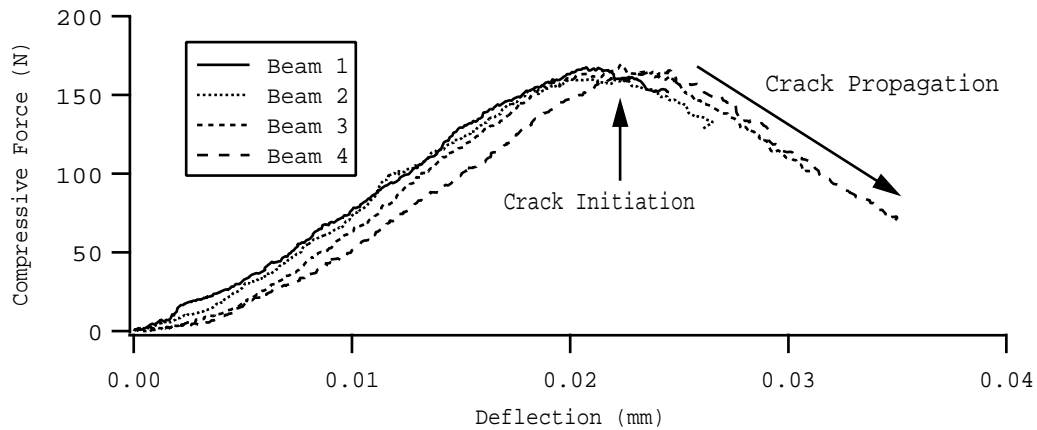


Figure 5. Force-deflection curves for cracked beam coupons during crack creation.

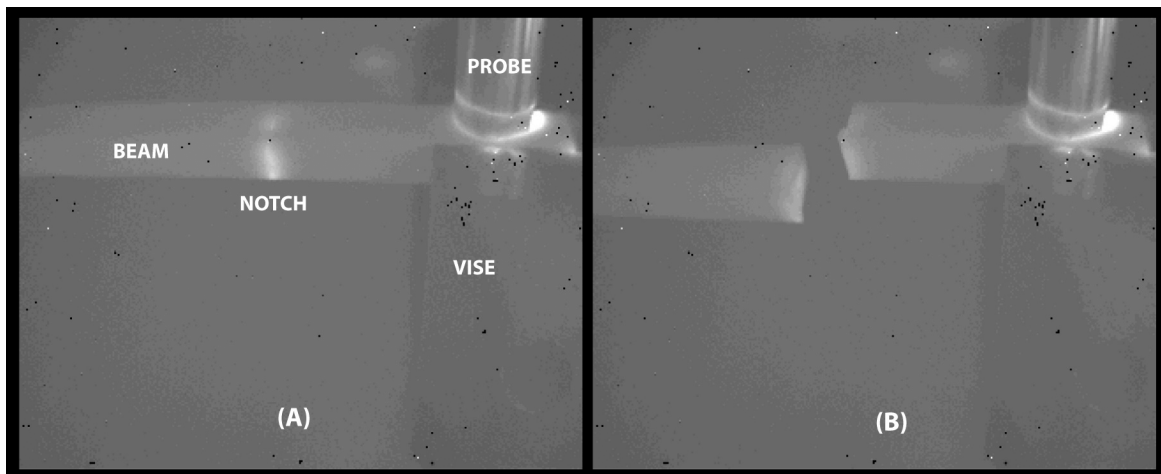


Figure 6. (A) Thermal signature from cracked beam coupon. (B) Eventual fracture of cracked beam coupon.

3.2. Carbon composite

The two tests on carbon composites were done on cured samples of graphite fiber in epoxy resin. One test was on tensile specimens that had been fatigued to failure in an MTS test machine. These tensile specimens had also been characterized by ultrasonic inspection, providing a useful comparison to another NDE technique. The tensile specimens also showed some dependence on the contact location of the probe. The other test was on a large thin square of composite that had been improperly bagged during vacuum forming. This specimen was tested on a variety of supports, showing the dependence on the thermal image to the support.

3.2.1. Tensile specimens

Four tensile specimens were tested with similar results. A typical tensile specimen is shown in Figure 7A. It consists of a midsection of composite, with two grips glued on the ends for mounting in the test machine. The ultrasonic image of the damaged midsection is shown in Figure 7B, where the light areas indicate damage. Two Sonic IR images are shown in Figures 7C and 7D. The thermal images are oriented correctly for comparison with the ultrasonic image. In general, the thermal images are in excellent agreement with the ultrasonic image, and show damage at the same locations. This good agreement with ultrasonic inspection was true of the other tested tensile specimens as well.

The Sonic IR results provided sharper images than the ultrasonic inspection. Notably, the early transients of the thermal image showed remarkable small detail as heat was produced at the damage interfaces. As the heat diffused from the damage site, the images became blurry and the detail was lost. However, the full transient response was available for review.

Some dependence on the probe contact location is noted as the differences between Figures 7C and 7D. Figure 7C shows the response when the probe contacts the left grip, while Figure 7D shows the response with the probe on the right grip. The right grip contact has generally stronger thermal images in this case. The other tensile specimens had similar results, in that the probe contact location would highlight or attenuate certain damage areas.

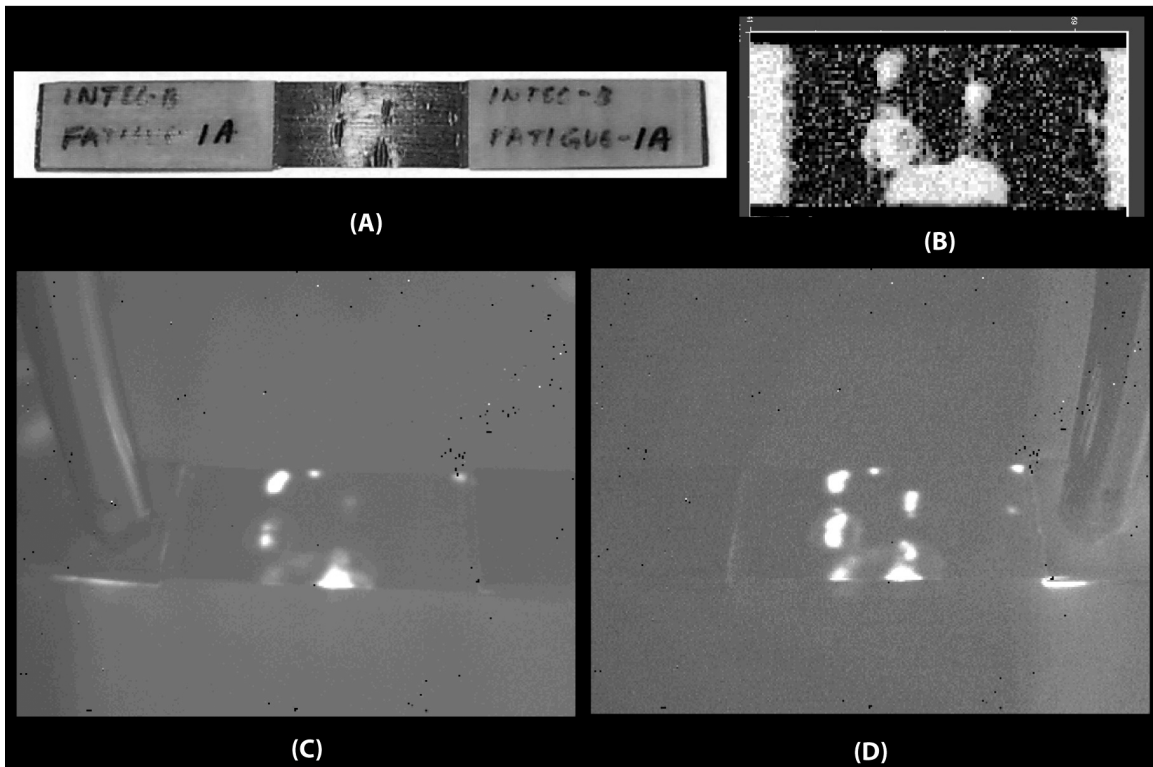


Figure 7. (A) Photograph of tensile specimen. (B) Ultrasonic image of damage. (C) Sonic IR image, probe at left grip. (D) Sonic IR image, probe at right grip.

3.2.2. Composite square.

The test object was a thin square of composite, 30 cm x 30 cm x 0.05 cm. The sample had a vacuum bagging failure during fabrication, resulting in poor bonding between fiber and matrix. The thermal image of damage should reflect the $\pm 45^\circ$ fiber plies over the entire surface. While attempting to image the damage, it was found that the thermal response of this object was strongly affected by the backing support.

The first attempt had the object resting on the ThermoSoniX test bed, which is a thin rubber mat over aluminum channel sections. No damage images were detected with this support, perhaps due to the rubber mat absorbing the energy through the thin composite. Next, the square was supported on an aluminum plate for backing. The thermal image for this support is shown in Figure 8A, and shows the expected $\pm 45^\circ$ orientation of damage, although localized at the probe rather than completely covering the object. Next, the square was supported on a smaller (15cm x 15 cm) tile of boron carbide, a dense stiff ceramic. The thermal image for this support is shown in Figure 8B. In this case, the thermal image appears to indicate dynamic coupling between the composite and the ceramic tile, but not any damage. The pattern of warm spots suggests a resonant modal response where the composite and the tile are rubbing together. The edges of the smaller tile underneath the composite square are evident in the thermal image as the perimeter of the warm spots, which further indicates that the two parts are dynamically coupled and causing the thermal signature.

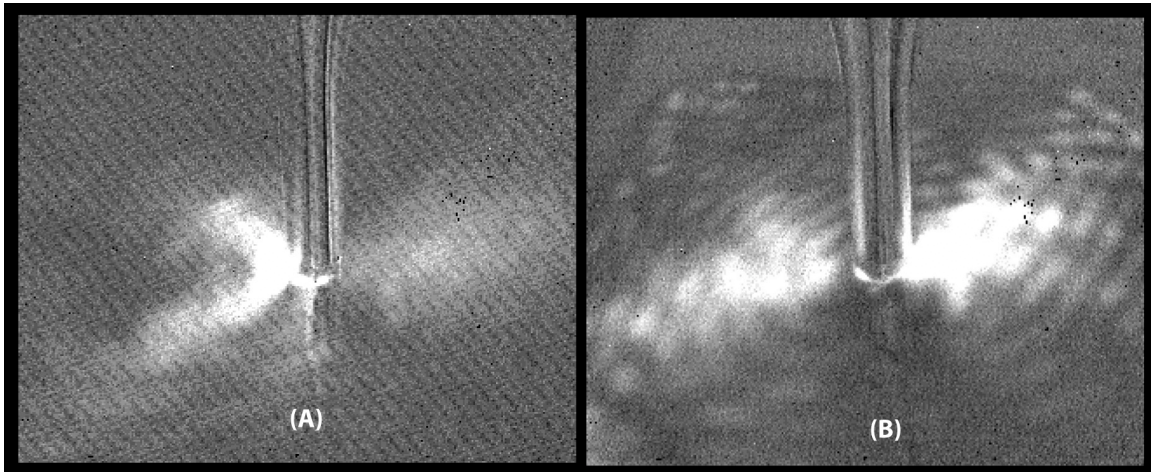


Figure 8. (A) Composite square on aluminum plate backing. (B) Composite square on small tile

3.3. Laser glass

A piece of laser glass with spallation pits from laser damage was tested. The glass was approximately 1 cm thick, and had many pits on the surface. The pits were typically 2 - 5 mm in diameter and half as deep. The walls of the pit were irregular fracture zones, and it was expected that the many small cracks left behind would produce thermal images at each pit. The glass was placed on the ThermoSoniX test bed rubber mat. Only several of the largest pits produced any detectable thermal images. Figure 9 shows the best image, where only one pit is clearly visible. Other pits were barely detectable and are not obvious in the image.

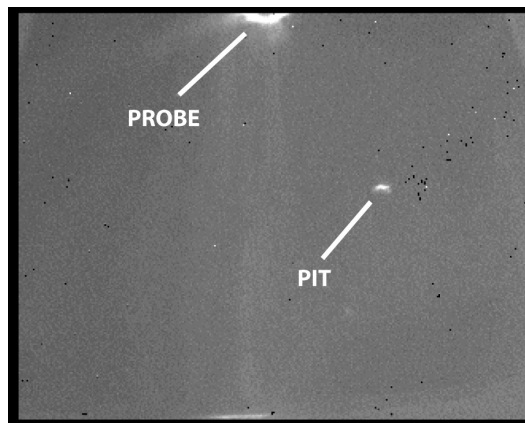


Figure 9. Thermal image from laser glass with spallation pits.

3.4. Steel

Tests were performed on several steel targets used to stop high-energy projectiles fired from the LLNL single-stage gas gun. The targets are characterized by large plastic deformations in the penetration zone, and some brittle fracture is also likely to be present. All of the targets produced thermal images at the penetration zone. The most interesting target is shown in Figure 10A. This is a cross section of a penetration zone, showing that a cylindrical plug from the target sheared away from the main body. The shear lines are clearly evident in the Sonic IR image, Figure 10B.

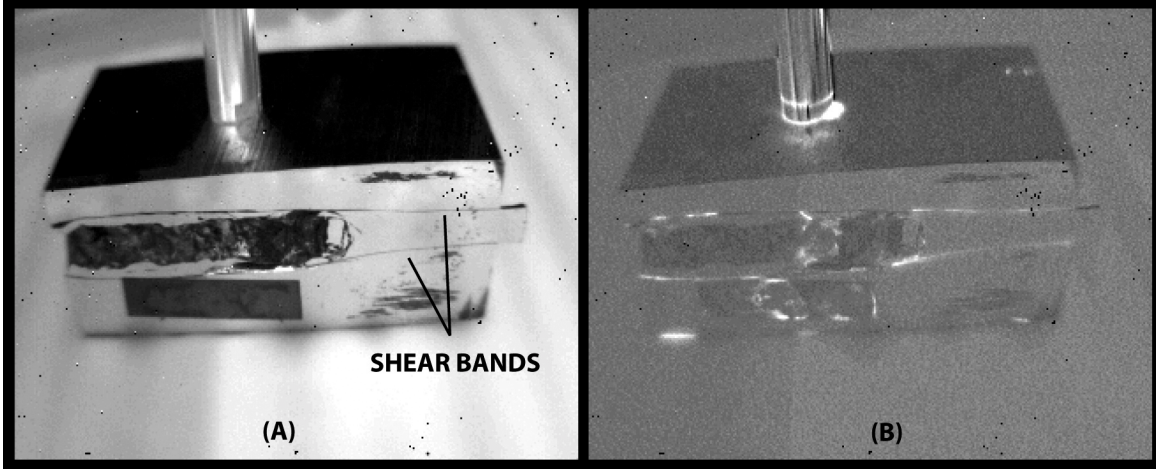


Figure 10. (A) Section view of target showing plug and shear bands. (B) Sonic IR image with illuminated shear bands.

4. DYNAMICS ANALYSIS

Sonic IR works because kinetic energy generated at the probe is transferred to the part, where it is converted into thermal energy by friction at a flaw and by material damping in bulk. Additionally, kinetic energy is transferred from the part to any fixtures or supports used to hold it, and these components may significantly alter the dynamic response of the part. A thorough knowledge of the method will require understanding how the energy transfer from probe to part to support takes place, and how the part dynamically responds, particularly the response at the flaw. More work is needed to complete these answers, however some aspects have been considered.

4.1. General development.

In the simplest case, consider a single spring-mass system, the classic harmonic oscillator. The governing equation is

$$\frac{d^2x}{dt^2} + \omega x(t) = f(t), \quad (1)$$

where $x(t)$ is displacement and $f(t)$ is the forcing input. The system has a resonant frequency $\omega = (k/m)^{1/2}$, where k is the spring stiffness and m is the mass. Allow the forcing to be harmonic with frequency ω_f so that $f(t) = P \sin(\omega_f t)$. The general solution is

$$x = X_H \sin(\omega t + \phi) + \frac{X_P}{1 - r^2} \sin(\omega_f t). \quad (2)$$

The first term is the homogeneous (unforced) solution with amplitude X_H . The second term is the particular (forced) solution with amplitude $X_P/(1 - r^2)$, where $r = \omega_f/\omega$. The constant angle ϕ is the phase lag between the two solutions. The functional forms of X_H and X_P can be found in any standard text on vibrations.⁷

Two observations on Eq. (2) are relevant. First, the solution consists of two sinusoids, one at the natural frequency and one at the forcing frequency. Thus the system is responding in both a natural mode and a forced response. Second, the amplitude of the forced response increases to infinity as $r \rightarrow 1$ ($\omega_f \rightarrow \omega$), which means that the system is being driven at resonance. More generally, the amplitude increases as the forcing frequency approaches a natural frequency.

Next, consider a continuous system rather than a single degree of freedom oscillator. The response of a continuous system varies in both space in time, $w(x,t)$, where $w(x,t)$ is the displacement. The natural response of a continuous system is defined by the eigenmodes, $\psi_n(x)$, and the associated eigenfrequencies, ω_n . This is the generalization of natural response to a continuous system with an infinite number of natural modes. The motion of a drumhead after being struck is a classic example of the superposition of eigenmodes, each responding at its eigenfrequency.

The overall response of a continuous system again consists of both homogeneous and particular solutions, $w(x,t) = w_H(x,t) + w_P(x,t)$. Thus the motion is a combination of eigenmodes ringing at the eigenfrequencies, and also a forced response responding to the input frequency. Again, forced resonance is possible if the forcing frequency approaches one of the eigenfrequencies. Moreover, the forcing input can be described as weighted integral of eigenmodes over the body, and the response as a weighted sum of eigenmodes. Using a modal expansion for the forced input and response provides

$$Q_n = \int f(t)\psi_n(x)dx \quad (3)$$

$$w_p(x,t) = \sum_{n=1}^{\infty} q_n(t)\psi_n(x) \quad (4)$$

where $q_n(t)$ are the generalized coordinates, which are the unknowns, and Q_n is the generalized force for the n^{th} degree of freedom. These are standard results, and are referenced in many texts on vibration and dynamics.⁸

Regarding Sonic IR, Eqs. (3) - (4) motivate the idea that the forced dynamic response of the part being excited must be considered as depending on both the input forcing, and also on the natural response of the system. In other words, the dynamic response will be different if changes are made to the geometry, the material or the input forcing, which is an intuitive result. Whether or not such changes will make a significant impact on the production of a thermal signature must be answered on a case-by-case basis. The results of this study suggest that this is so. Certainly the input frequency has an effect on the response. It would be interesting to consider broad-band input or a frequency sweep input to obtain a wider range of response.

4.2. Aluminum oxide study

To complete this initial investigation into the dynamics of Sonic IR, analyses of the natural response of the Vickers bit coupon and the cracked beam coupon were carried out to help explain the observed behavior. Recall that the Vickers bit coupon failed to produce a detectable thermal signature despite having visible closed cracks, while the cracked beam coupon provided a strong thermal signature but also broke readily under testing. The findings presented below suggest that the Vickers bit coupon didn't respond due to the high stiffness of the material, and the cracked beam coupons broke due to resonant forcing.

In a continuous system, Young's modulus, E , plays the same role as the spring stiffness in adjusting the eigenfrequencies. Increasing the modulus stiffens the part and raises the eigenfrequencies accordingly. Consequently, a part of aluminum oxide ($E=390$ GPa) will have much higher natural frequencies than the same part in aluminum alloy ($E=70$ GPa). This may help explain the failure to detect any thermal signature in the Vickers bit coupon.

A modal analysis of the Vickers bit coupon was done using a finite element model of similar proportions, which included a "plus-shaped" crack extending partway through the thickness. This crack geometry was considered as a simplified representation of the actual crack shown in Figure 3. The modal analysis computed the lowest 20 eigenmodes and eigenvalues of the cracked part. The fundamental (lowest) frequency was 15 kHz, and the highest computed frequency was 84 kHz. The mode shapes were then visually examined to pick the modes most conducive to creating heat by friction. These were identified by modes that caused rubbing at the crack faces. The dominant crack rubbing modes were found at frequencies of 61 kHz and 75 kHz. As shown in Figure 11, the 61 kHz mode was a vertical shearing motion of the crack faces and the 75 kHz mode was a lateral shearing motion. As these frequencies are well above the 20 kHz input frequency of the ThermoSoniX system, it is likely that they were not energized and that consequently there was no mechanism to create heat by friction at the crack.

For comparison, the modal analysis was repeated but using the properties of aluminum, which is more compliant than aluminum oxide. In this case, the range of frequencies was 7kHz – 42 kHz, half that of the aluminum oxide. Crack rubbing modes for aluminum were found at frequencies of 18kHz and 32 kHz, less than half those of aluminum oxide and

much closer to the 20 kHz input. Had the coupon been of aluminum, it is expected that the crack rubbing modes would have been energized and thermal signatures obtained.

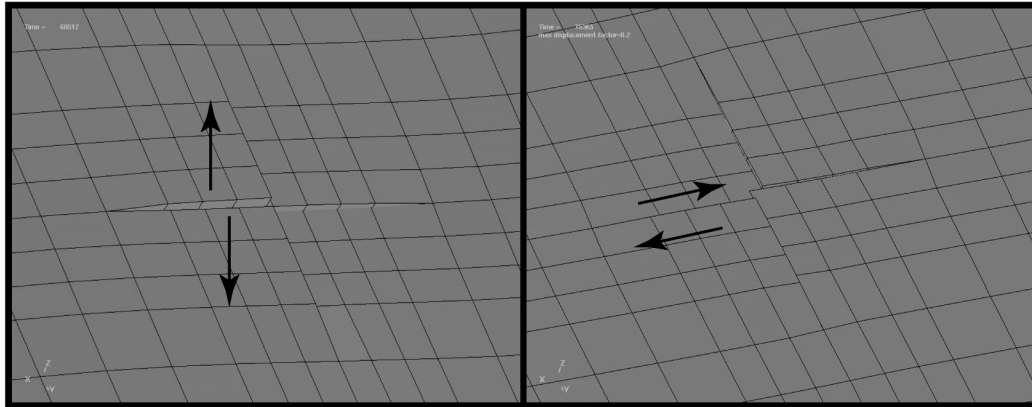


Figure 11, Vickers mode shapes at crack showing vertical shear at 61 kHz (left) and lateral shear at 75 kHz (right). Arrows indicate relative motion on the left branch of the crack.

Another modal analysis was carried out for the cracked beam coupon using a finite element model. The range of the twenty lowest natural frequencies was 300 Hz – 98 kHz. The dominant crack-rubbing frequency was at 19 kHz and is shown in Figure 12. This mode was also the closest in frequency to the 20 kHz input from the ThermoSoniX probe, suggesting that this mode was driven at resonance. This explains both the good thermal signature and the eventual breakage of the cracked beam coupons; the thermal signature was favored by a crack-rubbing mode driven to large amplitude, and the crack was further propagated by the same cause. It was coincidence that the best crack rubbing mode and the resonant mode were the same in this case.

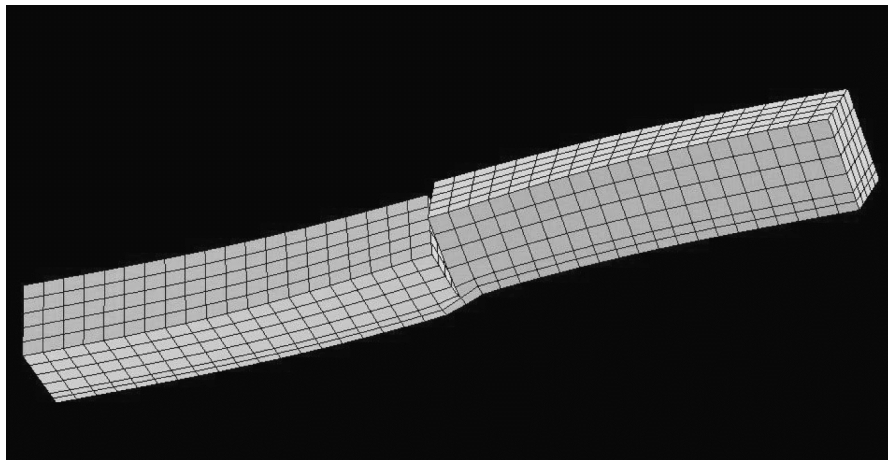


Figure 12. Cracked beam mode shape at 19 kHz showing crack-rubbing torsional motion.

5. CONCLUSIONS

Based on the results of this study, the following conclusions were made.

- (1) Sonic IR is a versatile and valuable new NDE technique that has application in a wide variety of circumstances. However, at this point the technique is not universally successful and not completely understood.
- (2) The ThermoSoniX system from Indigo Systems Corp. is a competent basic embodiment of Sonic IR that is intuitive and easy to use.
- (3) The dynamic response of a part being tested, and hence the thermal signature of the part, depends on the input forcing, the method of support, and the natural response of the part. All dynamically coupled components must work together to obtain valid thermal signatures of damage. Unsatisfactory coupling can lead to failure to obtain an image, or misleading images.
- (4) The excitation frequency should be matched to the natural response of the part to enhance heat-producing modes at flaws. A broadband frequency input or a frequency sweep would be useful as a general input.
- (5) Cracks can propagate and brittle parts can shatter from the input forcing. This may be due to forced resonance in some instances.
- (6) For some (notably thin) parts, the method of support is crucial in obtaining valid results. For other (notably thick) parts, the method of support is not crucial.

ACKNOWLEDGEMENTS

This work was performed under the auspices of the U.S. Department of Energy by Lawrence Livermore National Laboratory under Contract W-7405-Eng-48. The effort was completed with a great deal of help from many LLNL staff members, who provided expertise in materials science, manufacturing, laboratory assistance and samples for inspection. The author would also like to thank Sierra Olympic Technologies, Inc. and Indigo Systems Corp. for the rental, assistance and training with the ThermoSoniX equipment.

REFERENCES

1. Favro, L. D., Han, X., Ouyang, Z., Sun, G., Sui, H. and Thomas, R. L., "IR Imaging of Cracks Excited by an Ultrasonic Pulse," *Thermosense XXII, Proceedings of SPIE*, **4020**, pp. 182 - 185, 2000.
2. Farina, D. J., Richards, A., Han, X., "ThermoSoniX: A Novel Infrared- and Ultrasonic-Based System for Non-Destructive Testing built with LabVIEW, IMAQ Vision and DAQ," Indigo Systems Corp., Santa Barbara, CA, 2000.
3. Hockey, B. J. & Rice, R. W. (Eds.), *The Science of Ceramic Machining and Surface Finishing II*, NBS Special Pub 562, U.S. Govt. Printing Office, Washington, D.C., 1979.
4. Landingham, R. L., LLNL Ceramist (ret.), private communication, Nov. 2000.
5. Anstis, G.R., Chankikul, P., Lawn, B. R., & Marshall, D. B., "A Critical Evaluation of Indentation Techniques for Measuring Fracture Toughness: I, Direct Crack Measurements," *Journal of the American Ceramic Society*, **64**, No. 9, pp. 533 - 538, 1981.
6. Munz, D., Bubsey, R. T., & Shannon, J. L., "Fracture Toughness Determination of Al₂O₃ Using Four-Point-Bend Specimens with Straight-Through and Chevron Notches," *Journal of the American Ceramic Society*, **63**, No. 5 - 6, May - June 1980.
7. Vierck, R. K., *Vibration Analysis*, 2nd Ed., Harper & Row, New York, 1979.
8. Dowell, E. H. et al., *A Modern Course in Aeroelasticity*, Sijthoff & Noordhoff, The Netherlands, 1980.